Effect of Structure and Thermodynamic Stability on the Response of Lanthanide Stannate Pyrochlores to Ion Beam Irradiation

J. Lian,[†] K. B. Helean,[‡] B. J. Kennedy,[§] L. M. Wang,[†] A. Navrotsky,[‡] and R. C. Ewing*,[†]

Departments of Geological Sciences, Materials Sciences & Engineering, and Nuclear Engineering & Radiological Sciences, University of Michigan, Ann Arbor, Michigan 48109-1005, NEAT ORU and Thermochemistry Facility, University of California at Davis, Davis, California 95646-8779, and School of Chemistry F11, The University of Sydney, New South Wales 2006, Australia

Received: September 16, 2005; In Final Form: December 13, 2005

The lanthanide stannates, $Ln_2Sn_2O_7$, Ln = La−Lu and Y, have the isometric pyrochlore structure, $A_2B_2O_7$, and their structural properties have been refined by Rietveld analysis of powder neutron and synchrotron X-ray diffraction data. In this study, the enthalpies of formation of selected stannate pyrochlores, Ln = La, Nd, Sm, Eu, Dy, and Yb, were measured by high-temperature oxide melt solution calorimetry. Their radiation response was determined by 1 MeV Kr^{2+} ion irradiation combined with in situ TEM observation over the temperature range of 25 to 1000 K. The enthalpy of formation from binary oxides of stannate pyrochlores became more endothermic (from −145 to −40 kJ/mol) as the size of the lanthanide in the A-site decreases. A more exothermic trend of the enthalpy of formation was observed in stannate pyrochlores with larger lanthanide ions, particularly La, possibly as a result of increased covalency in the ⟨Sn−O⟩ bond. In contrast to lanthanide titanate pyrochlores, $Ln_2Ti_2O_7$, that are generally susceptible to radiation-induced amorphization and zirconate pyrochlores, $Ln_2Zr_2O_7$, that are generally resistant to radiation-induced amorphization, the lanthanide stannate pyrochlores show a much greater variation in their response to ion irradiation. La, Nd, and Gd stannates experience the radiation-induced transformation to the aperiodic state, and the critical amorphization temperatures are ∼960, 700, and 350 K, respectively. Y and Er stannate pyrochlores cannot be amorphized by ion beam irradiation, even at 25 K, and instead disorder to a defect fluorite structure. Comparison of the calorimetric and ion irradiation data for titanate, zirconate, and stannate pyrochlores reveals a strong correlation among subtle changes in crystal structure with changing composition, the energetics of the disordering process, and the temperature above which the material can no longer be amorphized. In summary, as the structure approaches the ideal, ordered pyrochlore structure, radiation-induced amorphization is more easily attained. This is consistent with an increasingly exothermic trend in the enthalpies of formation of pyrochlores from the oxides, that is, the greater the thermochemical stability of the pyrochlore structure, the more likely it will be amorphized upon radiation damage rather than recover to a disordered fluorite structure.

I. Introduction

The safe disposition of fissile Pu from dismantled nuclear weapons and the "minor" actinides (Np, Am, Cm) generated by the nuclear fuel cycle remain major challenges in developing strategies for advanced fuel cycles.[1] Recently, there has been great interest in using materials with fluorite and fluorite-related structures, such as pyrochlores, as potential host phases for the immobilization of actinides, particularly Pu.[2−10]

Pyrochlore, $A_2B_2O_7$ (A = La to Lu and Y; B = Ti, Zr, Sn), is isometric (*Fd*3*m*, $Z = 8$, $\boldsymbol{a} = 0.9$ to 1.2 nm) and closely related to the fluorite structure (AX_2), except that there are two cation sites and one-eighth fewer anions. The A-site at 16c is eight-coordinated and located within a distorted cubic coordination polyhedron, generally occupied by larger tri- and tetravalent actinides and lanthanides. The B-site at 16d is six-coordinated in a distorted octahedron and typically occupied by Ti, Zr, or Sn. There are two unique oxygen sites: The 48f oxygen is coordinated to two B^{4+} and two A^{3+} cations, while the 8b oxygen is in tetrahedral coordination with only A^{3+} cations. An unoccupied interstitial site, 8a, is surrounded by four B^{4+} ions, and the "vacancies" at the 8a site are ordered on the anion sublattice.[11−13] The oxygen at the 48f site is slightly displaced from that in the ideal fluorite structure ($x_{48f} = 0.3750$) toward the B-site cation. The magnitude of the displacement is measured by the value of the positional parameter, x_{48f}. Because all the atoms except the 48f oxygen are on special positions, the pyrochlore structure is completely described by the cubic lattice parameter, $\boldsymbol{a}$, and the 48f oxygen positional parameter, x (see refs 11 and 12). For $x = 0.3750$, the A-site coordination polyhedron is a regular cube, and the B-site polyhedron is distorted to a trigonally flattened octahedron (the topology of the fluorite structure). In this case, materials have a defect fluorite structure, and the occupancy of each anion site is 0.875. For $x = 0.3125$, the B-site is a regular octahedron, and materials have an ideal pyrochlore structure.

The advantage of using pyrochlore compositions, $A_2B_2O_7$, as potential waste forms is related to their remarkable compositional diversity and structural flexibility. Significant amounts

* Corresponding author. E-mail: rodewing@umich.edu.
[†] University of Michigan
[‡] University of California at Davis.
[§] The University of Sydney.

10.1021/jp055266c CCC: $33.50
Published on Web 01/13/2006

TABLE 1: Structural Parameters (Å) of Lanthanide Stannate Pyrochlores Obtained from Neutron and X-ray Diffraction Refinements of Pyrochlore Samples[26]

compositions	A^{3+} ionic radius	r_A/r_B	lattice parameter	$O_{48f}x$ parameter	$\langle A-O_{8b}\rangle$ bond length	$\langle A-O_{48f}\rangle$ bond length	$\langle Sn-O_{48f}\rangle$ bond length
$La_2Sn_2O_7$	1.160	1.681	10.7026	0.3294	2.317	2.629	2.074
$Nd_2Sn_2O_7$	1.109	1.607	10.5671	0.3322	2.288	2.576	2.06
$Sm_2Sn_2O_7$	1.079	1.564	10.5100	0.3330	2.2756	2.554	2.054
$Eu_2Sn_2O_7$	1.066	1.545	10.4753	0.3338	2.268	2.54	2.048
$Gd_2Sn_2O_7$	1.053	1.526	10.4544	0.3348	2.265	2.537	2.048
$Tb_2Sn_2O_7$	1.04	1.507	10.4235	0.3356	2.257	2.516	2.047
$Dy_2Sn_2O_7$	1.027	1.488	10.3979	0.3372	2.251	2.499	2.05
$Y_2Sn_2O_7$	1.019	1.477	10.3723	0.3369	2.246	2.495	2.043
$Ho_2Sn_2O_7$	1.015	1.471	10.3726	0.3366	2.246	2.497	2.042
$Er_2Sn_2O_7$	1.004	1.455	10.3504	0.3375	2.2401	2.485	2.042
$Tm_2Sn_2O_7$	0.994	1.440	10.3262	0.3382	2.236	2.475	2.04
$Yb_2Sn_2O_7$	0.985	1.428	10.3046	0.3391	2.231	2.4633	2.0398
$Lu_2Sn_2O_7$	0.977	1.416	10.2917	0.3397	2.2282	2.4559	2.0401

of actinides can be incorporated into the A-site of the pyrochlore structure. Radiation damage from α-decay events of the incorporated radionuclides may cause microstructural changes, macroscopic swelling, and a decrease in the chemical durability of the waste form[14] and may affect its long-term performance. Many studies [15−22] simulated the α-decay damage in a wide variety of pyrochlore compositions using ion beam irradiation, particularly in the systems $A_2Ti_2O_7$ and $A_2Zr_2O_7$.[15,16,19−23] Remarkably, pyrochlore structures display a wide range of behaviors in response to ion beam irradiation as a function of composition. Generally, titanate pyrochlores can be amorphized at relatively low doses (e.g., ∼0.2 displacements per atom (dpa) at room temperature for $Gd_2Ti_2O_7$).[16,20] However, a study of $Gd_2Ti_{2-x}Zr_xO_7$ showed a systematic increase in the "resistance" to ion beam induced amorphization with increasing zirconium content,[15,23] and the end-member pyrochlore $Gd_2Zr_2O_7$ remains crystalline at a dose of ∼36 dpa under 1.5 MeV Xe^+ irradiation at $T = 25$ K.[19] This result highlights the important effect of the B-site cation on the radiation response of pyrochlore materials. Although zirconate pyrochlores are generally considered to be radiation resistant, $La_2Zr_2O_7$ can be amorphized at room temperature by a 1.5 MeV Xe^+ ion irradiation at a dose of ∼5.5 dpa, but the critical amorphization temperature, T_c, is low, ∼310 K. Similar results of the critical amorphization dose and critical temperature for $La_2Zr_2O_7$ have been reported recently by 1 MeV Kr^{2+} ion irradiations.[24] Systematic ion beam irradiations of rare-earth titanate pyrochlores have demonstrated the importance of structure and bond type on the radiation "susceptibility" of pyrochlore as a function of the A-site cations.[20]

A systematic study of thermochemical properties has been completed by Helean et al.[25] using high-temperature oxide melt solution calorimetry on the series $Ln_2Ti_2O_7$ (Ln = Sm to Lu). All lanthanide titanates are stable in enthalpy with respect to their oxides: $Lu_2Ti_2O_7$ was the least stable (−56.0 ± 4.0 kJ/mol), and the most stable are Gd, Eu, and $Sm_2Ti_2O_7$ (−113.4 ± 2.7, −107.0 ± 4.1, −115.4 ± 4.2 kJ/mol, respectively). In general, as the radius ratio of the A- to B-site cation decreases, the pyrochlore structure becomes less stable, in part because the structure more closely resembles the defect fluorite structure; thus, it is energetically easier to disorder cations on the A- and B-sites. The energetics of the disordering process has important implications for the relative "resistance" of pyrochlore to radiation-induced amorphization. The "resistance" to radiation damage is considered to increase if a higher dose (i.e., displacements per atom) is required to cause disordering to the fluorite structure or radiation-induced amorphization. Another measure of "resistance" is the critical amorphization temperature, T_c, the temperature above which the material cannot be amorphized. Materials with a lower T_c are considered to be more radiation "resistant", because they recover from the damage at lower temperatures. Critical amorphization temperatures, T_c, vary over a rather large range, between 400 K (for $Lu_2Ti_2O_7$) to 1100 K ($Gd_2Ti_2O_7$), depending on the A-site cation. A remarkably consistent trend has been observed between the critical temperatures for amorphization and the enthalpies of formation of titanate pyrochlores from the oxides.[25] The more exothermic the enthalpy of formation, the higher the critical amorphization temperature is under 1 MeV Kr^{2+} ion irradiation.[20,25]

In the present paper, we report new data for the radiation response to 1 MeV Kr^{2+} ion irradiation and the energetics of formation of lanthanide stannate pyrochlores, $Ln_2Sn_2O_7$. The stannates form a complete series of isometric pyrochlore compositions, and the ionic radius ratio of A-site to B-site cations, r_{RE}/r_{Sn4+}, varies from 1.42 ($Lu_2Sn_2O_7$) to 1.68 ($La_2Sn_2O_7$). The thermochemistry of selected stannate pyrochlores $A_2Sn_2O_7$ (A = La, Nd, Sm, Eu, Dy, and Yb) was measured by high-temperature oxide melt solution calorimetry, and the enthalpies of formation of these stannates from their binary oxides were derived. The structural properties of the compounds under investigation have been well-characterized using Rietveld refinement of neutron diffraction and X-ray powder diffraction data.[26] These results provide insight into the relation of chemical composition to structural variations, enthalpies of formation, and the radiation response, e.g., the critical temperature for amorphization, of the pyrochlore compositions.

II. Experimental Section

II. A. Sample Synthesis and Characterization. Polycrystalline samples of stannate pyrochlores were synthesized by the solid-state reaction of SnO_2 with the appropriate trivalent oxides. The detailed synthesis was described in a previous study.[26] X-ray diffraction (XRD) was used to monitor the synthesis process and to confirm that the pyrochlore structure had formed with no detectable impurities. The structural parameters were determined in the previous study using Rietveld refinement based on powder neutron diffraction data for $Ln_2Sn_2O_7$, with Ln = Y, La, Pr, Nd, Tb−Lu, and powder X-ray diffraction measurements of Sm, Eu, and Gd stannate pyrochlores (Table 1).[26] The cubic lattice parameters are in agreement with the values obtained earlier by Brisse and Knop.[27] A linear increase of the lattice parameter, ***a***, with increasing ionic radius of the lanthanides suggests that these oxides are simple ionic compounds.

In this study, the chemical compositions and structural data of the stannate pyrochlore powder samples provided by Kennedy et al.[26] were characterized by X-ray powder diffraction, electron microprobe, and transmission electron microscopy. X-ray

TABLE 2: Enthalpies of Drop Solution, ΔH_{ds},[a] for Cassiterite, SnO_2, RE_2O_3, and the Pyrochlore Samples, $RE_2Sn_2O_7$[25,35,36]

RE	ΔH_{ds} (kJ/mol) sesquioxides	$\Delta H_f{}^0$ (kJ/mol) elements	ΔH_{ds} (kJ/mol) pyrochlore	ΔH_{f-ox} (kJ/mol) pyrochlore	$\Delta H_f{}^0$ (kJ/mol) pyrochlore
Yb	61.4 ± 2.12	−1814.6 ± 8.5	206.67 ± 5.03	−37.99 ± 5.59	−3007.8
Dy	50.2 ± 1.56	−1863.1 ± 3.9	211.05 ± 2.35	−53.57 ± 3.06	−3071.9
Eu	42.2 ± 0.99	−1662.7 ± 3.8	220.70 ± 3.50	−71.22 ± 3.83	−2889.1
Sm	27.2 ± 2.97	−1823.0 ± 2.0	215.03 ± 2.46	−80.55 ± 4.04	−3058.8
Nd	14.2 ± 3.96	−1807.9 ± 1.0	218.76 ± 2.80	−97.28 ± 4.99	−3060.4
La	−29.3 ± 4.43[37]	−1793.7 ± 1.6	220.10 ± 1.66	−142.12 ± 4.88	−3091.0
SnO_2	53.64 ± 0.84	−577.6 ± 0.2			

[a] ΔH_{ds} values reported for the RE sesquioxides are calculated using measured solution enthalpies and calculated heat contents.[31,35−37] Errors are calculated as 2 standard deviations of the mean.

powder diffraction (XRD) data were collected using a Scintag PAD-V diffractometer with a Cu anode and an accelerating voltage of 45 kV over an angular range, $2\theta = 14°$ to 94° and a 0.02° step size with a dwell time of 7 s. Unit cell parameters were refined and compared to those previously reported for these samples[26] and were found to be identical within experimental uncertainty. The XRD patterns indicated that these powder samples were pyrochlore and contained no measurable impurities.

Quantitative chemical analyses were completed using a Cameca SX50 electron microprobe (EMPA) with wavelength-dispersive spectroscopy (WDS), an accelerating voltage of 20 kV, a probe current of 10 nA, and a spot size of 1 μm. Energy dispersive spectroscopy (EDS), backscattered electron imaging (BSE), and characteristic X-ray dot mapping were used to assess chemical homogeneity. A ZAF correction was applied to the WDS data using the Cameca SX50 software. All samples studied were determined to be compositionally homogeneous and stoichiometric within analytical error. The pyrochlore structures of synthesized stannate powder samples were confirmed by transmission electron microscopy using a JEOL 2010 F transmission electron microscope (TEM) with a field emission source operated at 200 kV. High-resolution TEM images were used to assess the crystallinity of the powder samples. The TEM samples were prepared as dispersed powders on holey-carbon Cu grids. All stannate samples were stable under 200 keV electron beam irradiation.

II. B. Calorimetry. High-temperature oxide melt solution calorimetry[28,29] was used to measure the drop solution enthalpies of the pyrochlore samples plus their binary oxide components in molten $2PbO{\cdot}B_2O_3$ solvent at 1078 K. A Tian-Calvet twin microcalorimeter was used, whose design and operation were described in detail elsewhere.[28,29] Prior to calorimetry, the powder samples were dried at 973 K for a minimum of 1 h. The lanthanide sesquioxide powders were dried at 1473 K, vacuum-sealed in a desiccator, and handled in an Ar-filled glovebox to prevent hydration and carbonation of these samples. Drop solution enthalpies, ΔH_{ds}, were measured by dropping pellets (~5 mg) of the powdered samples from room temperature into the solvent at the calorimeter temperature. Thus, these enthalpies consist of two components, the heat content of the sample, $\int_{298}^{1078} C_p\, dT$, and the heat of solution, ΔH_s at 1078 K. Argon was bubbled through the melt to stir it and aid in the dissolution of the pellets.[30] The calorimeter was calibrated using the heat content of α-Al_2O_3 (NBS certificate: standard reference material 720; April, 1982). The measured values of the drop solution enthalpies were used in appropriate thermodynamic cycles to calculate the enthalpies of formation from the oxides. Reference data for the binary oxides were used to calculate the enthalpies of formation from the elements (Table 2).[31]

II. C. Ion Beam Irradiation. The response of stannate pyrochlores $A_2Sn_2O_7$ (A = La−Lu and Y) to ion beam damage was investigated using 1 MeV Kr^{2+} ion irradiation. Ion irradiation and in situ TEM observations were performed using the IVEM-Tandem Facility at the Argonne National Laboratory over the temperature range from 25 to 973 K. During irradiation, the ion beam was aligned approximately normal to the sample surface. The ion flux is set to be 6.25×10^{11} ions/cm^2/s. To avoid concurrent electron beam irradiation damage, the electron beam was turned off during the ion irradiation. The crystalline-to-amorphous transformation was determined by intermittent observation of the selected-area electron diffraction (SAED) pattern with increasing fluence. The critical amorphization fluence (F_c), the fluence at which complete amorphization occurs, was defined as the fluence at which all of the diffraction maxima in the SAED patterns had disappeared. A number of different grains were monitored during ion irradiations, and final doses were obtained by averaging the experimental data of those grains. Errors are calculated as 1 standard deviation of the mean value. Ex situ HRTEM observations were performed to investigate the radiation damage effects in detail. The critical amorphization fluence, F_c, in ions per centimeter squared, was converted to critical dose for amorphization, D_c, in units of displacements per atom (dpa) using SRIM-2000 calculations,[32] assuming a displacement energy of ~50 eV for all atoms in stannates pyrochlores. This value is consistent with the experimental data of $La_2Zr_2O_7$ and $Y_2Ti_2O_7$ determined by time-resolved cathodoluminescence spectroscopy measurements.[33]

III. Results

III. A. Drop Solution Calorimetry. Drop solution experiments using a $2PbO{\cdot}B_2O_3$ solvent at 1078 K were conducted for SnO_2, RE_2O_3 where RE = La, Nd, Sm, Eu, Dy, Yb, and the corresponding pyrochlore samples (Table 2). The ΔH_{ds} data for the RE sesquioxides were previously reported and shown to be reliable through the application of multiple thermodynamic cycles and cross-checks.[34−37] The calorimetric data were used in thermodynamic cycles (Table 3) to calculate enthalpies of formation of the RE stannates from the oxides, $\Delta H_{f-ox}{}^0$ (kJ/mol) (Table 2). The standard enthalpies of formation, ΔH_f^0, were also calculated (Table 2).

III. B. Ion Beam Irradiation. Ion beam induced amorphization occurred in some of the stannate pyrochlore compositions. Figure 1 shows the sequence of SAED patterns of selected stannate pyrochlore compositions (Nd, Dy, Ho, and Er) irradiated at room temperature or 25 K. The SAED patterns show a gradual decrease in the intensity of the diffraction maxima and the appearance of a diffuse halo that is characteristic of the accumulation of amorphous domains. Table 4 summarizes the critical amorphization fluence (ions/cm^2) and doses (dpa) at various temperatures for Gd, Nd, and La stannates. The temperature dependence of critical amorphization dose of $A_2Sn_2O_7$ (A = La, Nd, Gd) irradiated by 1 MeV Kr^{2+} is shown in

TABLE 3: Thermochemical Cycles Used to Calculated Formation Enthalpies for the $RE_2Sn_2O_7$ Samples Both from the Oxides, ΔH_{f-ox}, and from the Elements, ΔH_f^0 [a]

ΔH_1	$RE_2Sn_2O_7$ (c, 298 K) → [RE_2O_3 + $2SnO_2$] (sln, 1078 K)
ΔH_2	RE_2O_3 (c, 298 K) → RE_2O_3 (sln, 1078 K)
ΔH_3	SnO_2 (c, 298 K) → SnO_2 (sln, 1078 K)
ΔH_4	2RE (c, 298 K) + $^3/_2O_2$ (g, 298 K) → RE_2O_3 (c, 298 K)
ΔH_5	Sn (c, 298 K) + O_2 (g, 298 K) → SnO_2 (c, 298 K)
ΔH_{f-ox}	$= -\Delta H_1 + \Delta H_2 + 2\Delta H_3 =$ [RE_2O_3 + $2SnO_2$] (c, 298 K) → $RE_2Sn_2O_7$ (c, 298 K)
ΔH_f^0	$= \Delta H_{f-ox} + \Delta H_4 + 2\Delta H_5 =$ [2RE + 2Sn] (c, 298 K) + $^7/_2O_2$ (g, 298 K) → $RE_2Sn_2O_7$ (c, 298 K)

[a] Data are reported in Table 2.

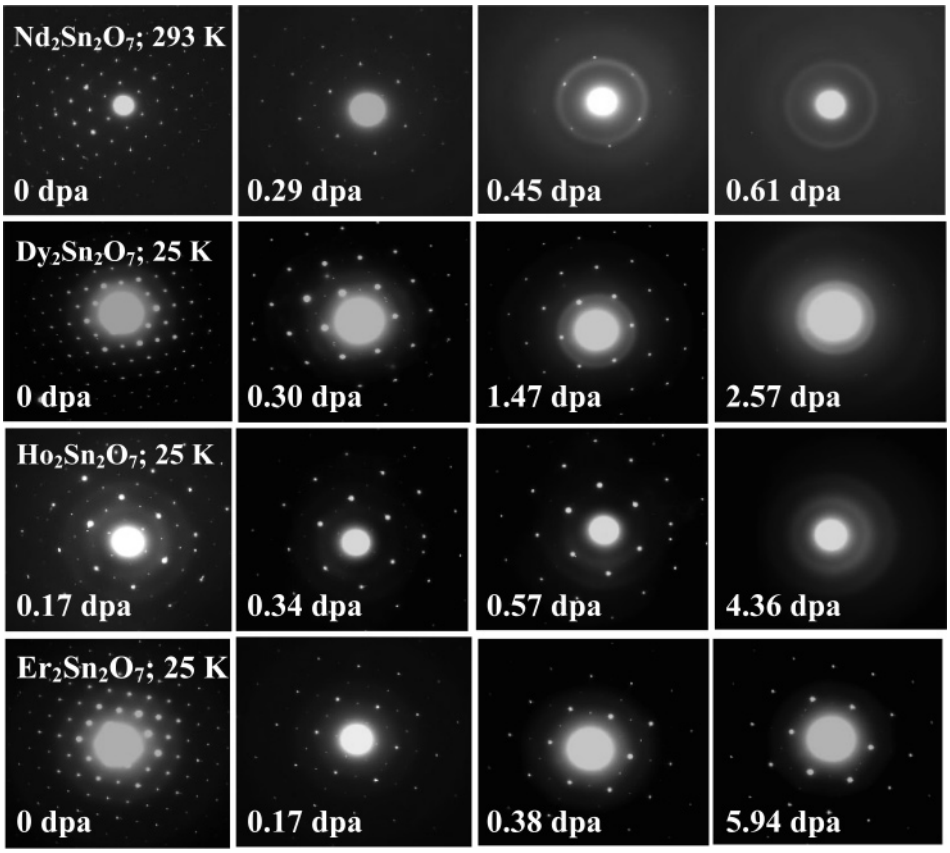

Figure 1. Sequence of selected-area diffraction patterns (SAED) of selected stannate pyrochlore compositions $A_2Sn_2O_7$ (A = Nd, Dy, Ho, Er) irradiated by 1 MeV Kr^{2+} ions at room temperature or 25 K. The corresponding ion doses are given with the SAED patterns.

TABLE 4: Summary of the Critical Amorphization Doses of La, Nd, and Gd Stannate Pyrochlores Subjected to 1 MeV Kr^{2+} Ion Irradiation[a]

	$La_2Sn_2O_7$		$Nd_2Sn_2O_7$		$Gd_2Sn_2O_7$	
temperature (K)	fluence (10^{14} ions/cm^2)	dpa	fluence (10^{14} ions/cm^2)	dpa	fluence (10^{14} ions/cm^2)	dpa
25			2.81 ± 0.25	0.37	6.52 ± 1.53	0.85
80	no data below				6.76 ± 1.35	0.88
200	room temperature				10.70 ± 0.76	139
293	2.5 ± 0.25	0.32	4.70 ± 0.31	0.61	26.2 ± 2.14	3.40
373			5.0 ± 0.31	0.65		
473	2.69 ± 0.19	0.34	5.63 ± 0.81	0.74		
573			6.25 ± 0.75	0.82		
673	3.88 ± 1.10	0.50	30 ± 1.25	3.92	no data above	
773	3.75 ± 0.63	0.48			room temperature	
823	5.63 ± 0.63	0.72	no data above 673 K			
873	6.09 ± 0.60	0.78				
973[b]	>25.0	>3.2				

[a] Errors are calculated as 1 standard deviation of the mean value. [b] No amorphization was observed at this dose.

Figure 2. The amorphization dose increases at higher irradiation temperatures, because dynamic annealing effects become more efficient in restoring crystallinity. The experimental data were modeled on the basis of the cascade quench model,[38] and the critical amorphization temperatures, above which the complete amorphization does not occur, were ~960, 700, and 350 K for $La_2Sn_2O_7$, $Nd_2Sn_2O_7$, and $Gd_2Sn_2O_7$, respectively.

By varying the chemical composition, the radiation response to ion beam irradiation of stannate pyrochlores changes significantly. Table 5 summarizes the critical amorphization dose

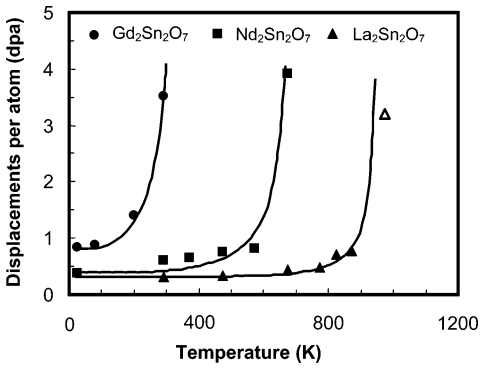

Figure 2. Temperature dependence of critical amorphization dose of stannate pyrochlores $A_2Sn_2O_7$ (A = La, Nd, and Gd) irradiated by 1 MeV Kr^{2+} ions.

TABLE 5: Summary of Radiation Response of Stannate Pyrochlores to 1 MeV Kr^{2+} Irradiation at 25 and 293 K[a]

	25 K (1 MeV Kr^{2+})		293 K (1 MeV Kr^{2+})	
composition	fluence (10^{14} ions/cm^2)	dpa	fluence (10^{14} ions/cm^2)	dpa
$La_2Sn_2O_7$			2.50 ± 0.25	0.32
$Nd_2Sn_2O_7$	2.81 ± 0.25	0.37	4.70 ± 0.31	0.61
$Eu_2Sn_2O_7$			11.3 ± 1.25	1.41
$Gd_2Sn_2O_7$	6.52 ± 1.53	0.81	26.2 ± 2.14	3.40
$Dy_2Sn_2O_7$	21.9 ± 2.5	2.57		
$Ho_2Sn_2O_7$	31.3 ± 3.13	4.36		
$Y_2Sn_2O_7$[b]	>47.5	>5.18	>62.5	>6.82
$Er_2Sn_2O_7$[b]	>43.8	>5.94	-	-

[a] Errors are calculated as 1 standard deviation of the mean value. [b] No amorphization was observed for $Y_2Sn_2O_7$ and $Er_2Sn_2O_7$.

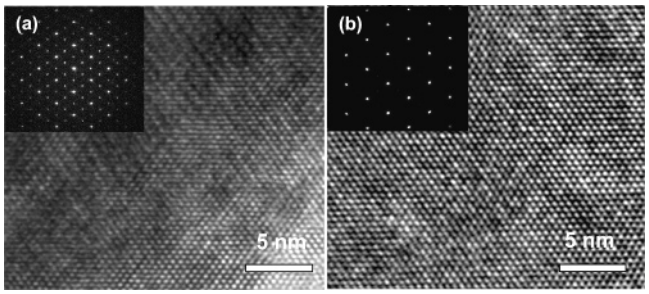

Figure 3. HRTEM images and selected-area diffraction patterns of $Y_2Sn_2O_7$: (a) unirradiated; (b) irradiated by 1 MeV Kr^{2+} at a dose of 6.25×10^{15} ions/cm^2 (~6.82 dpa) at room temperature. No evidence of amorphization was observed. The pyrochlore-to-fluorite structural transformation occurs in ion-irradiated $Y_2Sn_2O_7$.

for different stannate pyrochlores subjected to 1 MeV Kr^{2+} ion irradiation at 25 K and room temperature. $Er_2Sn_2O_7$ and $Y_2Sn_2O_7$ exhibited high "resistance" to ion beam induced amorphization, and no evidence of amorphization was observed for irradiation at room temperature and 25 K (~6.82 dpa) (Figure 3). An order−disorder pyrochlore-to-fluorite structural transition occurred in all ion-irradiated stannate pyrochlores, similar to that observed in titanate and zirconate pyrochlores.[13,15,19,20] For $Nd_2Sn_2O_7$, this transition occurred concurrently with amorphization (Figure 1). In contrast, the ion beam induced defect fluorite structure persisted for $Er_2Sn_2O_7$ with no subsequent amorphization observed. This order−disorder structural transition is also evidenced in the HRTEM images of $Y_2Sn_2O_7$ irradiated by 1 MeV Kr^+ at an ion fluence of 6.25×10^{15} ions/cm^2 (~6.82 dpa) (Figure 3).

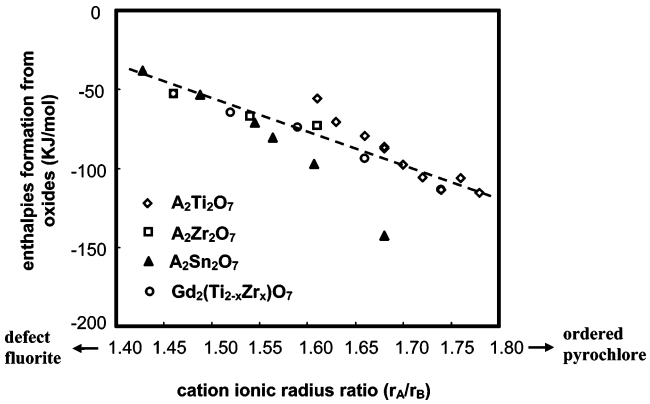

Figure 4. The enthalpy of formation from the oxides, ΔH_{f-ox}^0, of stannate pyrochlores vs the cation ionic radius ratio. All pyrochlores are stable relative to an oxide assemblage with increasing stability as the size of lanthanide elements increases. The enthalpies of formation from the oxides of titanate and zirconate pyrochlores were included for comparison.

IV. Discussion

IV. A. Formation Enthalpies. The formation enthalpies from oxides for stannate pyrochlores are plotted as a function of ionic radius ratio (Figure 4). Values are compiled in Table 2 together with the calculated standard formation enthalpies. All of the lanthanide stannate pyrochlores have exothermic enthalpies of formation with respect to their constituent oxides (Figure 4). With increasing cation ionic radius ratio (i.e., a relative increase in the size of the A-site cation), the formation enthalpies from oxides become more negative, consistent with the increased stability of the pyrochlore structure as the ionic radius ratio increases. Similar trends have been observed for lanthanide orthophosphates, $LnPO_4$,[39] alkali rare-earth double phosphates,[40] as well as titanate[25] and zirconate pyrochlores.[41] The enthalpies of formation of titanate and zirconate pyrochlores from the binary oxides are also included in Figure 4 for comparison. Generally, a linear trend was observed between the enthalpies of formation with the ionic radius ratio for a given tetravalent B-site cation (e.g., Ti, Zr, or Sn). Thus, for the stannate, titanate, and zirconate pyrochlores, all become more stable energetically as the lanthanide in the A-site becomes larger and the structure approaches that of the ideal ordered pyrochlore ($x_{48f} = 0.3125$). However, for the lanthanide stannates, the slope, the change in the enthalpy of formation as a function of ionic radius ratio, is much steeper than for the titanates or the zirconates.

There is an increased deviation from the linear behavior between enthalpy of formation of stannate pyrochlores and cation ionic radius ratio for the larger lanthanides, particularly for La^{3+}, in which the formation enthalpy of $La_2Sn_2O_7$ from the oxides is significantly more exothermic than suggested by the linear extrapolation of the data for other titanate, zirconate, and stannate pyrochlores (Figure 4). Bond-valence sum (BVS) calculations[26] indicate an increasing degree of covalency in the ⟨Sn−O⟩ bond as the ionic radius of the lanthanides increases, as evidenced by the decrease in the bond valence sum for Sn^{4+}, V_{Sn}. This increase in the covalency of the ⟨Sn−O⟩ bond is greatest for the larger lanthanides, especially La^{3+}, in which the V_{Sn} is less than 4.0. In contrast, the BVS for lanthanide ions increases from 2.616 in $Lu_2Sn_2O_7$ to 3.095 in $La_2Sn_2O_7$. The increased covalency of the ⟨Sn−O⟩ bond and ionic character of the ⟨Ln−O⟩ bond result in an increase in stability of the $La_2Sn_2O_7$ pyrochlore, as shown by the more negative formation enthalpy from the oxides (Figure 4). One can view this extra stabilization as arising from the difference in bond types between

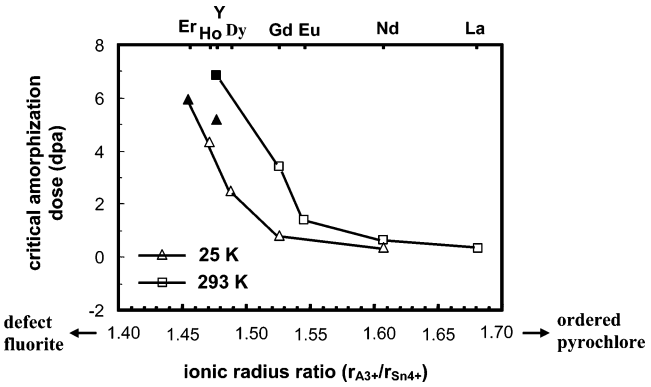

Figure 5. The critical amorphization dose of stannate pyrochlores irradiated by 1 MeV Kr^{2+} ions at 25 K or room temperature as a function of the cation ionic radius ratio. Solid symbols indicate that amorphization does not occur upon ion irradiation.

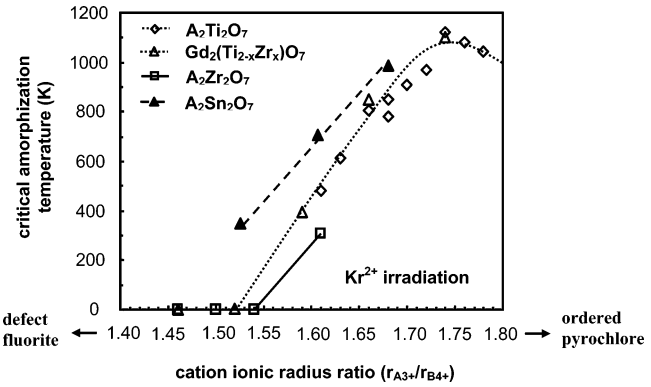

Figure 6. The critical amorphization temperature of stannate pyrochlore irradiated by 1 MeV Kr^{2+} as a function of the cation ionic radius ratio.[2] The data of titanate and zirconate pyrochlores are included for comparison (after ref 2).

La and Sn; as the La−O bond is longer and more ionic than for larger lanthanides, the covalent Sn−O bond can become stronger. The oxygen between Sn and La thus becomes more polarized, allowing greater electron density buildup in the more covalent Sn−O bond and leading to stabilization. These results provide evidence that bond type has an important effect in determining the structural trends and energetics of stannate pyrochlores; however, first-order variations in structure and formation enthalpies are mainly controlled by the relative sizes of the A- and B-site cations.

IV. B. Radiation Response. Generally, titanate pyrochlores $A_2Ti_2O_7$ (A = Lu−La and Y) are sensitive to ion beam damage, and the critical amorphization temperature varies significantly from 450 K (for $Lu_2Ti_2O_7$) to 1100 K ($Gd_2Ti_2O_7$) under 1 MeV Kr^{2+} irradiation.[20,42] Zirconate pyrochlores $A_2Zr_2O_7$ (A = Gd, Nd, and Eu) are "radiation resistant" to ion beam induced amorphization, as indicated by the higher temperatures, T_c, to which the radiation-induced aperiodic state persists. In contrast, the stannate pyrochlores display a wide range of responses to ion beam irradiations. La, Nd, and Gd stannates are sensitive to ion beam induced amorphization, and the critical amorphization temperature can be as high as 960 K (for $La_2Sn_2O_7$, 1 MeV Kr^{2+} irradiation), while other stannate pyrochlores form the disordered fluorite structure rather than becoming aperiodic, e.g., ion irradiations, even at 25 K, result in a disordered fluorite structure in $Er_2Sn_2O_7$ and $Y_2Sn_2O_7$.

The critical amorphization doses of $Ln_2Sn_2O_7$ with varying A-site cations subjected to 1 MeV Kr^{2+} ion irradiations at two baseline temperatures (293 and 25 K) are plotted in Figure 5 as a function of ionic radius ratio (r_{Ln3+}/r_{Sn4+}). With decreasing ionic radius ratio, the critical amorphization dose for both the 25 K and room-temperature irradiation increases, suggesting a decreased susceptibility to ion beam induced amorphization. Similarly, the critical amorphization temperature, T_c, decreases from 960 K for $La_2Sn_2O_7$ to 350 K for $Gd_2Sn_2O_7$, suggesting a significantly enhanced capability of defect recovery as the cation ionic radius ratio r_{Ln3+}/r_{Sn4+} decreases from 1.68 ($La_2Sn_2O_7$) to 1.526 ($Gd_2Sn_2O_7$). Energy-minimization calculations[3] have suggested that the cation antisite defect is the most stable defect in the pyrochlore structure. As the A-site cation radius approaches that of the B-site cation radius, the material is more likely to adopt the fluorite structure type. "Radiation resistance" reflects the balances between two competitive processes: the damage itself and the recovery to a crystalline structure. The former, producing highly displaced atoms and local amorphization, probably does not depend strongly on the nature of the lanthanide. The latter does, particularly if a relatively stable disordered but crystalline fluorite structure can form. When such a structure is favored, i.e., when the pyrochlore itself approaches the ideal cubic nondistorted structure, ready annealing of the initially amorphous domains to the crystalline disordered fluorite structure confers "radiation resistance".

The amorphization dose at 25 K for $Y_2Sn_2O_7$ is slightly higher than expected on the basis of the data for the lanthanide stannates. Although Y^{3+} (0.1019 nm) is slightly larger than Ho^{3+} (0.1015 nm), $Y_2Sn_2O_7$ has a higher "resistance" (i.e., a higher critical dose for amorphization) to ion beam induced amorphization than $Ho_2Sn_2O_7$. The critical amorphization dose of $Ho_2Sn_2O_7$ irradiated by 1 MeV Kr^{2+} at 25 K is 4.36 dpa, while $Y_2Sn_2O_7$ cannot be amorphized with a dose of 4.75×10^{15} ions/cm^2 (5.18 dpa) at 25 K and 6.25×10^{15} ions/cm^2 (~6.82 dpa) at room temperature (Table 5). This deviation for $Y_2Sn_2O_7$ is consistent with the structural trend, because $Y_2Sn_2O_7$ is closer to the ideal fluorite structure, as evidenced by the greater value for the O_{48f} positional parameter, x, as compared with $Ho_2Sn_2O_7$ (Table 1). Thus, $Y_2Sn_2O_7$ favors a disordered, defect fluorite structure upon ion irradiation.

Figure 6 summarizes the critical amorphization temperatures of all pyrochlore compositions subjected to 1 MeV Kr^{2+} ion irradiation as a function of the cation ionic radius ratio. Again, with the decreasing ionic ratio, the critical amorphization temperature generally decreases. However, the critical amorphization temperatures of stannate pyrochlores are much higher than those of titanate and zirconate pyrochlores having similar ionic radius ratios. For example, the cation ionic radius ratio of $La_2Sn_2O_7$ and $Y_2Ti_2O_7$ is 1.68; however, the critical amorphization temperatures of $La_2Sn_2O_7$ and $Y_2Ti_2O_7$ with 1 MeV Kr^{2+} irradiations are 960 and 780 K, respectively. The critical amorphization temperature of $Nd_2Sn_2O_7$ is 700 K, significantly higher than that of $Lu_2Ti_2O_7$ (480 K), although the ionic radius ratio of $Nd_2Sn_2O_7$ ($r_{Nd3+}/r_{Sn4+} = 1.607$) is slightly less than that of $Lu_2Ti_2O_7$ ($r_{Lu3+}/r_{Ti4+} = 1.61$). This deviation for stannate pyrochlores from the ionic size trend for titanates and zirconates is further evidenced by the comparison between the radiation responses of $Gd_2Sn_2O_7$ and $Gd_2(Zr_{0.75}Ti_{0.25})_2O_7$ in terms of critical amorphization dose at 25 K. Although the cation radius ratio of $Gd_2Sn_2O_7$ (~1.526) is similar to that of $Gd_2(Zr_{0.75}Ti_{0.25})_2O_7$ (~1.523), there is a dramatic difference in the radiation "resistance" (see Figure 6). No amorphization occurs in $Gd_2(Zr_{0.75}Ti_{0.25})_2O_7$ with an ion irradiation at 25 K, whereas $Gd_2Sn_2O_7$ can be amorphized at room temperature at a dose of ~3.4 dpa.

This more complex behavior of stannate pyrochlores may reflect different cation electronic configurations and variation

in bond type. The covalent character of the ⟨Sn−O⟩ bond of stannate pyrochlores implies a lesser degree of distortion of the SnO_6 coordination octahedron, resulting in a structure more compatible with the ordered pyrochlore superstructure.[26] This leads to a greater susceptibility of stannate pyrochlore to ion beam irradiation induced amorphization, as compared with the titanate and zirconate pyrochlores with similar ionic radius ratios. First-principle calculations[43] using density functional theory have reported a significant covalency for the ⟨Sn−O⟩ bond and mainly ionic character for the ⟨Ti−O⟩ and ⟨Zr−O⟩ bonds. The covalency of the ⟨Sn−O⟩ bonds has also been observed in a maximum entropy method electron density study of $Y_2Sn_2O_7$.[44] The greater degree of covalent bonding between ⟨Sn−O⟩ as compared with ⟨Ti^{4+}−O⟩ or ⟨Zr^{4+}−O⟩ results in greater defect formation energies than otherwise predicted.

Naguib and Kelly[45] correlated the radiation tolerance of nonmetallic solids with the relative ionicity of the material, finding that more covalently bonded materials sustain greater amounts of damage (that is, they are more readily amorphized) at lower temperatures under heavy ion irradiation. For example, they compared the ionicities of SnO_2, TiO_2, and ZrO_2, and predicted that SnO_2, because of its greater covalency, would be more susceptible to amorphization. Eby et al.[46] noted that complex silicates with a greater proportion of ⟨Si−O⟩ bond are more susceptible to radiation-induced amorphization. More recently, Trachenko[47] has developed a new criterion for evaluating the response of complex nonmetallic materials to radiation-induced amorphization. He defines "resistance" to amorphization as a competition between long-range and short-range forces originating from the ionic and covalent contributions to bonding. Short-range covalent forces are expected to dominate and stabilize the disordered damage area by increasing the energy barriers for local rearrangement processes, while the long-range forces reduce the energetic barriers in more ionic materials, leading to increased ease of recrystallization of the disordered domains. Using this criterion, Trachenko[47] analyzed the resistance to amorphization of 116 materials including titania, silicates, perovskite, and pyrochlore. For the $Gd_2(Ti_{1-x}Zr_x)_2O_7$ binary system, the increasing radiation "resistance" to amorphization is attributed to the reduced contribution of the short-range covalent forces resulting from the ⟨Ti−O⟩ bonds as the content of Zr increases. Similarly, the greater degree of the covalency of the ⟨Zr−O⟩, ⟨Hf−O⟩, and ⟨Sn−O⟩ bonds account for the higher "radiation resistance" of $La_2Zr_2O_7$ [19,22,24] and $La_2Hf_2O_7$[24] as compared with $La_2Sn_2O_7$.

However, the bond type criteria of Naguib and Kelly[45] and Trachenko[47] do not explain the radiation response of all pyrochlore compositions. This is because there are subtle structural changes, slight changes in bond length, that occur with changes in the bond type of A- and B-site cations. The current experimental data demonstrate that stannate pyrochlore compositions exhibit a significantly greater variation in their response to irradiation, i.e., "resistance" to amorphization, than would be anticipated from the criteria of Naguib and Kelly [45] or the short-range forces that originate from the covalency of the ⟨Sn−O⟩ bond. For example, the ⟨B−O⟩ bond of $Y_2Sn_2O_7$ is significantly more covalent than that of $Y_2Ti_2O_7$ or $Y_2Zr_2O_7$, as evidenced by the electronic density maps obtained by first-principle calculation.[43] On the basis of the bond type criteria of Naguib and Kelly[45] and Trachenko,[47] $Y_2Sn_2O_7$ should display a greater susceptibility to ion beam induced amorphization than $Y_2Ti_2O_7$. However, $Y_2Sn_2O_7$ is one of the most radiation resistant pyrochlores and shows no evidence of amorphization at a dose of 6.82 dpa at room temperature.

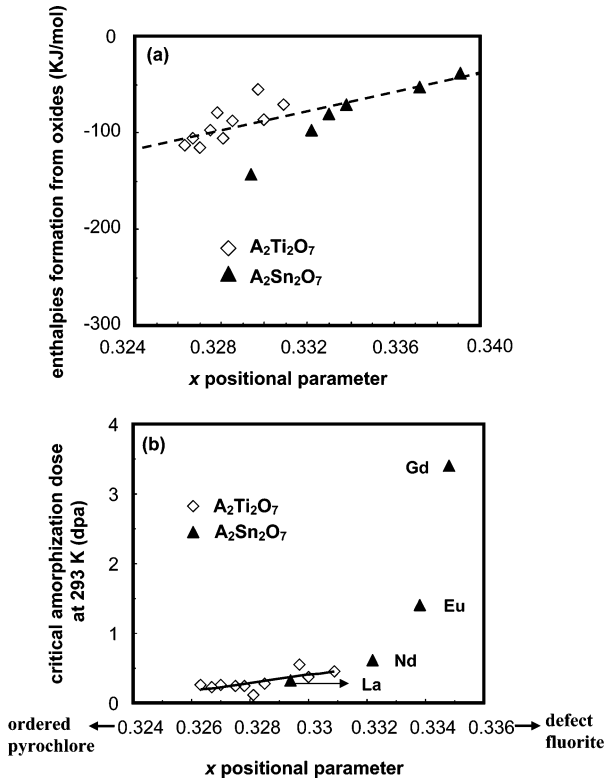

Figure 7. (a) The enthalpies of formation from oxides of stannate and titanate pyrochlores as a function of 48f oxygen positional parameter, *x*. (b) The change in the critical amorphization doses of titanate and stannate pyrochlores irradiated by 1 MeV Kr^{2+} ions at room temperatures as a function of 48f oxygen positional parameter, *x*.

IV. C. Structural Trends, Enthalpies of Formation, and Radiation Response. The experimental results in this paper clearly demonstrate that the enthalpies of formation from oxides and the radiation response behavior of pyrochlore compounds are highly composition dependent, and the cation ionic radius ratio plays a dominant role in both. However, some deviations from the ionic radius ratio trends (Figures 5 and 6) were observed for both the enthalpies and radiation susceptibility to ion beam induced amorphization. These deviations can be attributed to the combined effects of the cation electronic configuration and bond type. The cation ionic radius ratio and bond type both affect the cation polyhedra distortion, hence the structural deviation from the ideal fluorite structure, as represented by 48f oxygen positional parameter, *x*. Figure 7a shows the enthalpies of formation from the oxides of titanate and stannate pyrochlores as a function of 48f oxygen position parameter, *x*. Generally, the enthalpies of formation become more endothermic with increasing *x* values as materials approach the ideal fluorite structure, except for stannates with larger lanthanides at the A-site, such as $La_2Sn_2O_7$. The critical amorphization doses at room temperature of titanate and stannate pyrochlores are plotted in Figure 7b as a function of 48f oxygen positional parameter, *x*. The critical ion doses for amorphization generally decrease as the structure approaches that of the ideal pyrochlore. A similar behavior is also observed for the critical amorphization temperature of titanate pyrochlores. As the pyrochlore structures approaches the ideal fluorite structure with a higher *x* value (e.g., stannate pyrochlores from $La_2Sn_2O_7$ to $Gd_2Sn_2O_7$), the critical amorphization doses increase significantly, and some materials (e.g., $Y_2Sn_2O_7$ and $Er_2Sn_2O_7$) cannot be amorphized at room temperature by ion beam irradiation. These results demonstrate the relation between the pyrochlore structure and the enthalpies of formation of pyrochlore com-

pounds and the radiation susceptibility to ion beam induced amorphization. We have previously reported the remarkable consistency between the measured enthalpy of formation from oxides and the "resistance" to radiation damage as measured by the critical amorphization temperature of titanate pyrochlores $A_2Ti_2O_7$.[25] The generally increasing radiation "resistance" to amorphization from titanate, stannate, to zirconate pyrochlores is consistent with the decreasing pyrochlore superstructure stability, as indicated by the less exothermic trend in the enthalpies of formation from oxides.

V. Conclusions

$Ln_2Sn_2O_7$, Ln = La−Lu and Y, form a complete series of isometic pyrochlore structures. The formation enthalpies of stannate pyrochlores and their "resistance" to the radiation-induced transformation to the aperiodic state were investigated by high-temperature oxide melt solution calorimetry and ion beam irradiation, respectively. Structural variations in pyrochlore (i.e., radius ratio of the A- and B-site cations and the bond type) were correlated to the enthalpy of formation, the critical dose for amorphization, and the critical temperature for radiation-induced amorphization. All of the lanthanide stannate pyrochlores are stable in their enthalpy of formation with respect to their oxides. The lanthanide stannate pyrochlores show a much wider range of radiation responses than either the titanate or zirconate pyrochlores. Gd, Nd, and La stannate pyrochlores are susceptible to ion beam damage, while Y and Er stannate pyrochlores cannot be amorphized by ion beam irradiation. There is a consistent correlation among the crystal structure, the enthalpy of formation, and the radiation "resistance" as characterized by the critical amorphization dose and temperature. The greater "resistance" to irradiation-induced amorphization for materials having structures closer to the ideal fluorite structure is consistent with the less exothermic trend in the enthalpies of formation from the oxides and the decreasing stability of isometric pyrochlore structure. These results document the strong correlation among the structure, energetics, and the radiation response of the different compositions of the pyrochlore structure type.

Acknowledgment. We are grateful to the staff of the IVEM-Tandem Facility at the Argonne National Laboratory for assistance during ion irradiation experiments. We are also very grateful for the thoughtful comments and great suggestions by an anonymous reviewer. This work was supported by the Office of Basic Energy Sciences, U. S. Department of Energy under DOE grants DE-FG02-97ER45656 and DE-FG03ER46053.

References and Notes

(1) Taubes, G. *Science* **1994**, *263*, 629.
(2) Ewing, R. C.; Weber, W. J.; Lian, J. *J. Appl. Phys.* **2004,** 95, 5949.
(3) Sickafus, K. E.; Minervini, L.; Grimes, R. W.; Valdez, J. A.; Ishimaru, M.; Li, F.; McClellan, K. J.; Hartmann, T. *Science* **2000**, *289*, 748.
(4) Weber, W. J.; Ewing, R. C. *Science* **2000,** *289*, 2051.
(5) Weber, W. J.; Ewing, R. C. *Mater. Res. Soc. Symp. Proc.* **2002**, *713*, 443.
(6) Helean, K. B.; Navrotsky, A.; Vance, E. R.; Carter, M. L.; Ebbinghaus, B.; Krikorian, O.; Lian, J.; Wang, L. M.; Catalano, J. G. *J. Nucl. Mater.* **2002**, *303*, 226.
(7) Digeos, A. A.; Valdez, J. A.; Sickafus, K. E.; Atio, S.; Grimes, R. W.; Boccaccini, A. R. *J. Mater. Sci.* **2003**, *38*, 1597.
(8) Raison, P. E.; Haire, R. G. *Prog. Nucl. Energ.* **2001**, *38*, 251.
(9) Shoup, S. S.; Bamberger, C. E.; Haire, R. G. *J. Am. Ceram. Soc.* **1996**, *79*, 1489.
(10) Begg, B. D.; Hess, N. J.; McCready, D. E.; Thevuthasan, S.; Weber, W. J. *J. Nucl. Mater.* **2001**, *289*, 188.
(11) Subramanian, M. A.; Aravamudan, G.; Rao, G. V. S. *Prog. Solid State Chem.* **1983**, *15*, 55.
(12) Chakoumakos, B. C. *J. Solid State Chem.* **1984**, *53*, 120.
(13) Lian, J.; Wang, L. M.; Wang, S. X.; Chen, J.; Boatner, L. A.; Ewing, R. C. *Phys. Rev. Lett.* **2001**, *87*, 145901.
(14) Weber, W. J.; Wald, J. W.; Matzke, Hj. *Mater. Lett.* **1985**, *3*, 173.
(15) Wang, S. X.; Begg, B. D.; Wang, L. M.; Ewing, R. C.; Weber, W. J.; Kutty, K. V. G. *J. Mater. Res.* **1999**, *14*, 4470.
(16) Wang, S. X.; Wang, L. M.; Ewing, R. C.; Was, G. S.; Lumpkin, G. R. *Nucl. Instrum. Methods Phys. Res. B* **1999**, *148*, 704.
(17) Begg, B. D.; Hess, N. J.; Weber, W. J.; Devanathan, R.; Icenhower, J. P.; Thevuthasan, S.; McGrail, B. P. *J. Nucl. Mater.* **2001**, *288*, 208.
(18) Lian, J.; Wang, L. M.; Ewing, R. C.; Boatner, L. A. *Nucl. Instrum. Methods Phys. Res. B* **2005**, *241*, 365.
(19) Lian, J.; Zu, X. T.; Kutty, K. V. G.; Chen, J.; Wang, L. M.; Ewing, R. C. *Phys. Rev. B* **2002**, *66*, 054108.
(20) Lian, J.; Chen, J.; Wang, L. M.; Ewing, R. C.; Farmer, J. M.; Boatner, L. A.; Helean, K. B. *Phys. Rev. B* **2003**, *68*, 134107.
(21) Lian, J.; Ewing, R. C.; Wang, L. M.; Helean, K. B. *J. Mater. Res.* **2004**, *19*, 1575.
(22) Lian, J.; Wang, L. M.; Haire, R. G.; Helean, K. B.; Ewing, R. C. *Nucl. Instrum. Methods Phys. Res. B* **2004**, *218*, 236.
(23) Wang, S. X.; Wang, L. M.; Ewing, R. C.; Kutty, K. V. G. *Mater. Res. Soc. Symp. Proc.* **1999**, *540*, 355.
(24) Lumpkin, G. R.; Whittle, K. R.; Rios, S.; Smith, K. L.; Zaluzec, N. J. *J. Phys. Condens. Matter.* **2004**, *16*, 8557.
(25) Helean, K. B.; Ushakov, S. V.; Brown, C. E.; Navrotsky, A.; Lian, J.; Ewing, R. C.; Farmer, J. M.; Boatner, L. A. *J. Solid State Chem.* **2004**, *177*, 1858.
(26) Kennedy, B. J.; Hunter, B. A.; Howard, C. J. *J. Solid State Chem.* **1997**, *130*, 58.
(27) Brisse, F.; Knop, O. *Can. J. Chem.* **1968**, *46*, 857.
(28) Navrotsky, A. *Phys. Chem. Miner.* **1977**, *2*, 89.
(29) Navrotsky, A. *Phys. Chem. Miner.* **1997**, *24*, 22.
(30) Navrotsky, A. *J. Therm. Anal. Calorim.* **1999**, *57*, 653.
(31) Robie, R. A.; Hemingway, B. S. *U. S. Geol. Surv. Bull.* **1995**, 2131.
(32) Ziegler, J. F.; Biersack, J. P.; Littmark, U. *The Stopping and Range of Ions in Solids*; Pergamon Press: New York, 1985.
(33) Smith, K. L.; Collela, M.; Cooper, R.; Vance, E. R. *J. Nucl. Mater.* **2003**, *321*, 19.
(34) Ushakov, S. V.; Helean, K. B.; Navrotsky, A.; Boatner, L. A. *J. Mater. Res.* **2001**, *16*, 2623.
(35) Helean, K. B.; Navrotsky, A. *J. Therm. Anal. Calorim.* **2002**, *69*, 751.
(36) Takayama-Muramchi, E.; Navrotsky, A. *J. Solid State Chem.* **1993**, *106*, 349.
(37) Cheng, J.; Navrotsky, A. *J. Mater. Res.* **2003**, *18*, 2501.
(38) Wang, S. X.; Wang, L. M.; Ewing, R. C. *Phys. Rev. B* **2001**, *63*, 024105.
(39) Ushakov, S. V.; Helean, K. B.; Navrotsky, A.; Boatner, L. A. *J. Mater. Res.* **2001**, *16*, 2623.
(40) Ushakov, S. V.; Navrotsky, A.; Farmer, J. M.; Boatner, L. A. *J. Mater. Res.* **2004**, *19*, 2165.
(41) Helean, K. B.; Navrotsky, A.; Ewing, R. C. Unpublished.
(42) Ewing, R. C.; Lian, J.; Wang, L. M. *Mater. Res. Soc. Symp. Proc.* **2004**, *792*, 37.
(43) Panero, W. R.; Stixrude, L. P.; Ewing, R. C. *Phys. Rev. B* **2004**, *70*, 054108.
(44) Ikeda, T.; Sakata, M.; Takata, M.; Kennedy, B. J.; Cookson, D. J.; Howard, C. J. *Jpn. J. Appl. Phys.* **1999**, *38*, 93.
(45) Naguib, H. M.; Kelly, R. *Radiat. Eff.* **1975**, *25*, 1.
(46) Eby, R. K.; Ewing, R. C.; Birtcher, R. C. *J. Mater. Res.* **1991**, *7*, 3080.
(47) Trachenko, K. *J. Phys.: Condens. Matter* **2004**, *16*, R1491.